8.8 Second Harmonic Generation and Nonlinear Raman Scattering

SHG is a new, high-resolution, nonlinear optical imaging modality for the study of intact tissues and cellular structures.[177, 1133, 1134, 1141, 1146, 1156, 1160, 1161, 1569, 1570–1573, 1575, 1577–1602] SHG is a second-order nonlinear optical process that can only arise from media lacking a center of symmetry, e.g., an anisotropic crystal, or at an interface such as membrane. It can be used to image highly ordered structural proteins without exogenous labels, as well as biological membrane probes with high membrane specificity.

Collagen, as a primary component of connective tissues, has an appreciable nonlinear susceptibility for SHG. The helix of collagen secondary structure is noncentrosymmetric, satisfying a condition for SHG, which self-assembles into higher order structures. Collagen has been shown to have a dominant uniaxial second-order nonlinear susceptibility component aligned along the fiber axis. In such multicomponent tissues as skin, SHG light is mostly generated within dermis, not cellular layers like epidermis or subcutaneous fat.

SHG techniques have many advantages connected with dividing of incident wavelength and selectivity to tissue structure, which allow one to easily reject surface reflection and multiple scattering of the incident light in the upper epithelial layer without using a gating technique. As in the case of multiphoton fluorimetry, excitation light is in the NIR wavelength range, which is not excessively strongly scattered by tissue, and the SHG signal is generated in a very small volume of tissue occupied by the focused laser beam. This provides high spatial resolution, acceptable in many cases for the in-depth probing and separation of excitation and detection signals. Tightly focused laser beams with high power density and very short pulse duration in the range of tens or hundreds of femtoseconds allow for the generation of harmonics in undamaged living tissue, due to the brief interaction of radiation with tissue and the low overall energy—less than that needed for ionization of molecules. In addition, SHG polarimetry is an effective tool to probe collagen orientation in tissues.[1575, 1576, 1578, 1579, 1600]

In general, the nonlinear polarization of a material can be expressed as[1571]

$$\mathbf{P} = \chi^{(1)}\mathbf{E} + \chi^{(2)}\mathbf{EE} + \chi^{(3)}\mathbf{EEE} + , \ldots , \tag{8.63}$$

where $\mathbf{P}$ is the induced polarization, $\chi^{(n)}$ is the nth order nonlinear susceptibility, and $\mathbf{E}$ is the electric field vector of the incident light. The first term describes normal absorption and reflection of light; the second, SHG, sum, and difference frequency generation; and the third, both two- and three-photon absorption, as well as third harmonic generation and coherent anti-Stokes Raman scattering (CARS).

SHG, by contrast to two-photon fluorescence (see Subsection 5.2), does not arise from an absorptive process. Instead, an intense laser field induces nonlinear, second-order polarization in the assembly of molecules, resulting in the production of a coherent wave at exactly twice the incident frequency (or half the wavelength). The spectral and temporal profiles of two-photon excited fluorescence and SHG are also different. For two-photon fluorescence, the width of the emission spectrum is determined by the relative geometries of the ground and excited molecular states,

and the emission lifetime is related to the oscillator strength of the transition and is typically on the order of a few nanoseconds. In SHG, by contrast, both the spectral and temporal characteristics are derived from the laser source: the bandwidth scales, as $1/\sqrt{2}$ times the bandwidth of the excitation laser; and, owing to the coherence of the process, the SHG pulse is temporally synchronous with the excitation pulse.

A simplified expression for SHG signal intensity has a form[1571]

$$I(2\omega) \propto \left[\chi^{(2)} \frac{E(\omega)}{\tau_p}\right]^2 \tau_p, \tag{8.64}$$

where $\chi^{(2)}$ is the second-order nonlinear susceptibility, $E(\omega)$ and τ_p are the laser pulse energy and width, respectively. As in two-photon fluorescence [see Eqs. (5.13)–(5.16)], the signal is quadratic with peak power, but because SHG is an instantaneous process, a signal is generated only during the duration of the laser pulse. The macroscopic value, $\chi^{(2)}$, can be expressed in terms of the first molecular hyperpolarizability, β, as

$$\chi^{(2)} = \rho_M \langle \beta \rangle, \tag{8.65}$$

where ρ_M is the density of molecules and the brackets denote orientational average. This underscores the need for a noncentrosymmetric region, because $\langle \beta \rangle$ would vanish for an isotropic distribution of dipole moments. It follows from Eqs. (8.64) and (8.65) that the SHG signal depends on the square of the molecular surface density, whereas the intensity of two-photon fluorescence is linear with the density of fluorophores [see Eq. (5.11)].

Within the two-level system model, β is given by[1571]

$$\beta = \frac{3e^2}{2\hbar^3} \frac{\omega_{ge} f_{ge} \Delta\mu_{ge}}{\left[\omega_{ge}^2 - \omega^2\right]\left[\omega_{ge}^2 - 4\omega^2\right]}, \tag{8.66}$$

where e is electron charge; $\hbar\omega_{ge}$, f_{ge}, and $\Delta\mu_{ge}$ are the energy difference, oscillator strength, and change in dipole moment between the ground and excited states, respectively. Although SHG is not an absorptive process, the magnitude of the SHG wave can be resonance-enhanced when the energy of the second harmonic signal overlaps with an electronic absorption band. It follows from Eq. (8.66) that β grows large when the fundamental frequency of the laser approaches the electronic transition; then, the total second-order response is a sum of the nonresonant and resonant contributions:

$$\chi^{(2)}_{total} = \chi^{(2)}_{nonres} + \chi^{(2)}_{res}. \tag{8.67}$$

Depending upon the specific properties of the molecule and the excitation wavelength, the resonant contribution can dominate, resulting in enhancement of an order of magnitude or more.

SHG microscopy has been successfully used to produce high-resolution images of living cells,[1571] 3D imaging of endogenous structural proteins in tissues,[1572] and biomolecular arrays in cells, tissues, and organisms.[1573] *In vivo*

dynamic imaging of collagen in normal tissues and in its modified state in the tumor is described in Ref. 1574, and the generation of polarized SHG images of collagen are discussed in Refs. 1575, 1576, 1579, and 1584, including images of rat tail tendon[1575] and dermis of human skin.[1579]

SHG microscopy allows one to study many biochemical and biophysical processes, such as collagen nanostructure by analyzing the susceptibility tensor of the second order;[1599] spatial orientation of the fibrous structures of tissues;[1600] structural changes in mixed collagen gels (types I and V) as a marker to record changes in human breast stroma with cancer;[1590] microstructural and mechanical properties of collagen gel;[1594] the mechanism of reversible dissociation of collagen in tissues under the influence of glycerol;[1578] the role of myosin in the formation of SHG signals from muscle sarcomeres;[1585] the twist angles of myosin and collagen;[1596] and the electrical activity in intact neural networks.[1591]

In Ref. 1591, the SHG excitation was provided by a high-powered fiber laser operating in the 1064-nm spectral range (see Fig. 8.32). The scanning head of the random access second-harmonic generation (RA-SHG) microscope was developed by using two acousto-optical deflectors (AODs) crossed at 90 deg. To compensate for the larger dispersion attributable to two crossed AODs, an acousto-optical modulator placed at 45 deg with respect to the two axes of the AODs was used. A microscope objective focused the excitation light into the tissue. The SHG signal was collected in the forward direction and detected with a GaAsP photomultiplier (PMT) module. Figure 8.32(b) presents an SHG image of rat cerebellar slice at three different depths of 10, 50, and 100 μm. Examples of SHG signals include those of a Purkinje cell (red arrow), granule cell (yellow arrow), and interneuron (blue arrow). These images were acquired with the same laser power across all three depths.

SHG, as a method of nonlinear multiphoton imaging, has considerable potential for clinical studies.[1597] For example, it is possible to quantify the status of a disease such as osteogenesis imperfect;[1587] to monitor the restructuring of the extracellular matrix in ovarian cancer;[1589] to visualize skin lesions;[1592] to quantitatively analyze the structure of collagen in the human dermis under healthy and pathological states;[1593] and to obtain images of the cornea after intrastromal femtosecond laser ablation.[1580]

The primary advantage of the nonlinear methods is that labeling is rarely needed; however, new types of markers, such as ZnO nanoparticles with a strong nonlinear response, can be useful, for example, in the study of nanoparticle diffusion in tissues and their use as local generators or quenchers of free radicals in the treatment or prevention of dental and skin diseases.[1157–1161] The SHG method with and without nanomarkers is a prospective technique for *in vivo* nonlinear cytometry.[173, 179, 182, 1147, 1152, 1155, 1156]

Because the SHG method is technically implemented by using similar experimental equipment to multiphoton fluorescence and CARS, these methods are often used together as part of a multimodal approach to gather more information about fundamental processes in tissues and cells (see for example, Refs. 1577, 1601, and 1602). CARS is formally described in terms of four-wave

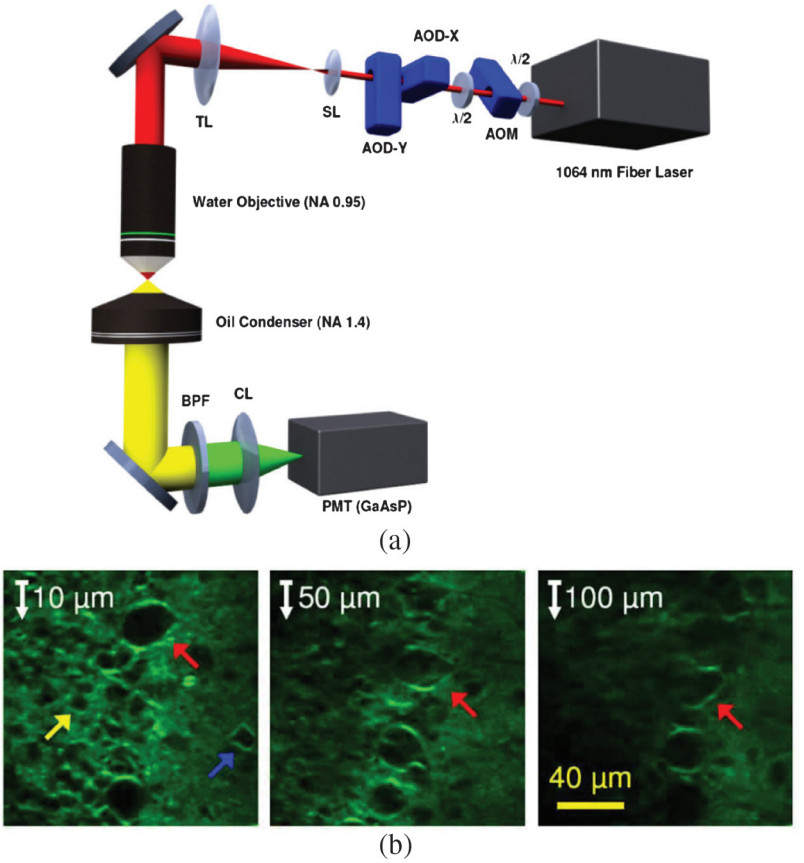

Figure 8.32 RA-SHG microscope (see Ref. 1591). RA-SHG microscope arrangement: a fiber laser ($\lambda = 1064$ nm) provided the excitation light, which comprised 200 fs width pulses at 80-MHz repetition rate. The laser beam was adjusted for optimal linear polarization via a half-wave ($\lambda/2$) plate. Beam passes were made through 45-deg AOM for angular spreading precompensation. A second half-wave ($\lambda/2$) plate was placed after the AOM to optimize the diffraction efficiencies of the two orthogonally mounted AODs: AOD-*x* and AOD-*y*. A scanning lens (SL) and a microscope tube lens (TL) expanded the beam before it was focused onto the specimen by the objective lens. The SHG signal was collected by an oil immersion condenser, band-pass filtered (BFP) and focalized by a collection lens (CL) into a GaAsP PMT (photomultiplier) (a). SHG image of rat cerebellar slice at three different depths of 10, 50, and 100 μm. Examples of SHG signals from a Purkinje cell (red arrow), granule cell (yellow arrow) and interneuron (blue arrow). The images were acquired with the same laser power across all three depths (b). (See color plates.)

mixing,[5,181,1171,1172,1601–1608] as indicated by the molecular vibrational state diagrams in Figs. 5.11 and 8.33. CARS is a third-order nonlinear optical process in which three excitation fields interact to produce a fourth field, which is detected. In general, two laser beams with frequencies ν_{pump} and ν_{S} are tuned to determine their difference, $\nu_{\text{pump}} - \nu_{\text{S}}$, to be equal to the frequency, ν_{vib}, of a vibrational transition of the sampling molecules. Then, the probing laser beam with frequency, ν_{probe}, resonantly generates a fourth enhanced field with frequency $\nu_{\text{AS}} =$

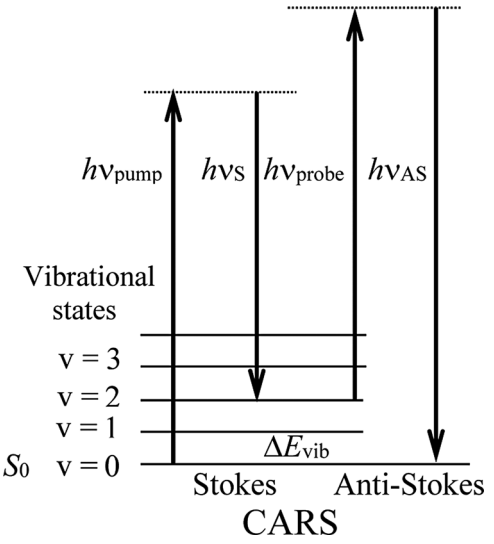

Figure 8.33 Molecular energy levels and transitions involved in the CARS process (see Ref. 181).

$\nu_{pump} + \nu_{vib}$. Figure 8.33 presents these transitions characteristic to the CARS process. Typically, only two laser beams are used to generate the CARS signal, because a so-called frequency-degenerate optical scheme with $\nu_{pump} = \nu_{probe}$ can be applied. The intensity of the CARS signal depends quadratically on the modulus of the induced third-order polarization, $\mathbf{P}^{(3)}$ in the sample [see Eq. (8.63)]:

$$I_{AS} \propto \left|\mathbf{P}^{(3)}\right|^2, \tag{8.68}$$

where $\mathbf{P}^{(3)}$ depends on the third-order optical susceptibility, which can be presented as a sum of the nonresonant and resonant contributions:

$$\mathbf{P}^{(3)} = \left[\chi^{(3)}_{nonres} + \chi^{(3)}_{res}\right] \mathbf{E}_{pump}\mathbf{E}_{probe}\mathbf{E}_S \tag{8.69}$$

The primary advantages of CARS compared to conventional Raman, in addition to the opportunity to amplify the signal by more than four orders of magnitude, are direct signal generation, narrow band, and a complete absence of the influence of AF because the signal is generated at wavelengths shorter than that of excitation. In Ref. 1577, the SHG method in combination with two-photon fluorescence allowed the authors to obtain *in vivo* images of cells and extracellular matrix. Investigation of the effect of DMSO on the dynamics of skin optical clearing by quantitative multimodal nonlinear microscopy (SHG/CARS) is presented in Ref. 1601; and simultaneous multimodal imaging for *in vivo* studies of the dynamics of biological processes, integrating multiplex coherent anti-Stokes Raman scattering (M-CARS), SHG, and two-photon fluorescence, is described in Ref. 1602.

When integrating with a laser scanning microscope, CARS can provide video images. The method was used for imaging and monitoring the lipid vesicles in

HeLa cells and membrane of lysed erythrocytes; growing fat droplets in living adipocytes; transporting organelles within living cells; and storing lipids in nematode *Caenorhabditis elegans* upon the registration of CARS signal at 2845 cm^{-1}.[1605] It was shown that CARS imaging is not destructive to cells under study if the measurement does not exceed 5 min.[1605]

Principles and prospects for development of CARS as a technique for noninvasively obtaining specific information about the chemical and molecular structure of an object without the use of exogenous markers and, and its biological and medical applications, are discussed in Refs. 1171, 1172, 1603, and 1604. *Ex vivo* study of mouse brain using M-CARS in comparison with results of the classical histological analysis confirmed the potential of the method as an ideal tool for chemoselective imaging in tissues.[1606] It is shown that the method enables quantitative analysis of CARS images, which is necessary, for example, for the real-time diagnosis of breast cancer.[1607] In particular, functional imaging of cell and tissue structures using CARS and corresponding image processing algorithms make it possible to distinguish cancerous lesions from normal tissue and benign proliferative lesions.

A commercially available micro-endoscope was used for minimally invasive multimodal nonlinear video imaging of cellular processes in the spinal cord of living mice.[1608] The system allows for obtaining CARS images of myelin sheaths and fluorescence detection at two-photon excitation from microglial cells and axons. Despite its small diameter, a micro-endoscope provides high-speed multimodal imaging in a sufficiently large region of tissue and with sufficient resolution to measure small differences in the thickness of the myelin sheaths and motility of microglial cells.

A typical probing depth of nonlinear microscopy and spectroscopy is less than 300 μm owing to the strong scattering of many tissues under study.[1609] However, the use of tissue optical clearing technology by replacing the water with other fluids having a similar refractive index to that of proteins[200, 201, 1609, 1612] can significantly reduce scattering and reach a probing depth greater than 2 mm. A more detailed description of the tissue optical clearing method is presented in the next chapter.

8.9 Terahertz Spectroscopy and Imaging

The terahertz frequency range, which occupies an intermediate position between the IR and microwave frequency ranges (1 THz → 1 ps → 300 μm → 33 cm^{-1} → 4.1 meV → 47.6 K) (see Fig. 8.34), is relatively less studied in the whole range of electromagnetic waves from radio to x-rays. Efficient sources of radiation have appeared only in the last two decades, primarily due to the development of lasers with ultrashort pulses. Excited by laser pulses, terahertz (THz) radiation is promising for applications in biology and medicine because of the following important features: (1) many vibrational transitions of biomolecules are found in this range; (2) the heterogeneity of tissues that causes strong scattering of electromagnetic radiation in the visible and NIR does not cause measurable scattering in the THz range; (3) the refraction of different types of tissues varies greatly; and (4)